NI PARTITIONING TO OXIC SEDIMENT: RAPID AND EFFICIENT REMOVAL OF NICKEL BY BEDDED SEDIMENT

Final report submitted to
Nickel Producers Environmental Research Association (NiPERA)

Prepared by
David Costello and Raissa Mendonca
Kent State University

April 2017
(updated Jan 2018)

Summary

Nickel bioavailability in sediment is modified by naturally occurring ligands that can complex Ni and reduce its toxicity. Many of the environmental quality standards for Ni in sediment consider reduced sulfur and organic matter as important modifying factors, but more recently Fe, Mn, and Al metal oxide minerals have been shown to alter sediment Ni bioavailability. We used controlled laboratory assays with five geochemically diverse sediments to study the binding of Ni to oxidized sediment ligands. Using a modification of OECD Test 308, we incubated field-collected surface sediment and buffered reconstituted freshwater solution (1:4 v:v ratio) with dissolved Ni (0.5, 2, or 5 mg L^{-1}) under different pH conditions (pH 5, 7, or 9) for 28 days. Ni concentrations in overlying water declined rapidly in most treatments, and frequently reached an equilibrium concentration within a few days. Slower Ni removal occurred when overlying water was pH 5 and when the mass of Ni added was low. At equilibrium, the sediment sorbed 44–100% of the added Ni, and approximately two thirds of the test conditions (i.e., sediment type × pH × Ni added) were predicted to remove >70% of the added Ni. Ni dynamics in the overlying water were strongly correlated to the dynamics of Ni sorbed to metal oxides as shown by selective extractions. Increased Ni removal (i.e., greater proportion of added Ni sorbed to sediment) was correlated to the affinity of Fe for Ni measured as both the Ni:Fe ratio in hydrous ferric oxide (HFO)-specific extractions and the Ni-HFO partitioning coefficient ($K_{Ni\text{-}HFO}$). Ni removal efficiency was negatively correlated with acid-volatile sulfide (AVS) and organic matter in sediment, which supports the hypothesis that metal oxides are the more important ligand for Ni in surface sediments. Although the specific affinity of metal oxides for Ni was strongly correlated with Ni removal from the water column, bulk mineralogical sediment characteristics (e.g., total Fe, total HFO) were either uncorrelated or negatively correlated with Ni removal. Particle size was positively correlated to Ni removal, which suggests that metal oxides on the surfaces of larger particles have greater affinity for Ni. These data show that Ni removal from overlying water by surface sediments is rapid and complete in non-acidic (i.e., pH > 6) conditions, and the completeness of Ni removal is related to properties of metal oxide minerals. We propose additional studies to (1) explore the properties of the metal oxide minerals that have the greatest affinity for Ni and (2) determine the reversibility of Ni sorbed to metal oxide minerals under changing environmental conditions.

Introduction

In aquatic ecosystems, nickel (Ni) can be toxic to organisms but its cycling and toxicity are coupled to other elemental cycles that can limit its bioavailability (Campbell and Tessier 1996, Chapman and Wang 1998). Current sediment quality benchmarks consider acid-volatile sulfide (AVS) as the major binding phase for Ni, but have not yet incorporated ligands that are present in oxic sediments. Although advances have been made in modeling metal partitioning in oxic sediments these approaches have not been integrated into risk assessment to the degree that AVS-based models have been. A growing body of literature emphasizes the importance of metal oxide minerals for sorbing toxic metals and reducing metal bioavailability (Costello et al. 2011, 2016). However, research on the behavior of metal partitioning onto metal oxide minerals, especially within the context of the mixture of competing ligands found in natural sediments, is warranted to derive information on binding coefficients (Tessier 1992). Our study aimed to collect empirical data on Ni partitioning to natural sediments ranging in geochemical properties

(1) as a foundation for risk assessment approaches for oxic sediment and (2) to demonstrate the dynamics of metal partitioning with oxic sediment particles, which can be used to calculate Ni removal rates.

Materials and methods

Sediment collection

Streams in Ohio were surveyed and selected for sediment collection based on geochemical characteristics. Selected stream sites included Tinkers Creek (TK), Breakneck Creek (BN), Plum Creek (PM), and Robinson Run (RR) in northeast Ohio and Little Sugar Creek (LS) and Little Miami River (LM) in southwest Ohio. All sediments were selected to have naturally low AVS and background sediment Ni concentrations but a wide range of total iron, total manganese, total aluminum, organic carbon content, and particle size (Tables 1 & 2). At each of the stream sites, surface sediment samples (5–10 cm deep; OECD 2002) were manually collected with a shovel into 1-gallon buckets. In the lab, sediments were wet sieved through a 2 mm mesh and stored in the fridge until the experimental setup.

Table 1. Summary of sediment chemistry

Initial sediment physicochemical characteristics from six Ohio streams (mean ± standard deviation)

Location	AVS (μmol g^{-1} dw)	Total Fe (mg kg^{-1} dw)	Crystalline Fe (mg kg^{-1} dw)	Amorphous Fe (mg kg^{-1} dw)	Total Mn (mg kg^{-1} dw)	Total Al (mg kg^{-1} dw)	Organic matter (%)
Tinkers Creek (TK)	1.57 ± 0.86	13,000 ± 300	5,400 ± 575	3,050 ± 360	517 ± 41	3,580 ± 75	3.1 ± 0.3
Plum Creek (PM)	2.41 ± 0.43	9,300 ± 700	4,000 ± 1,400	2,200 ± 320	268 ± 38	2,900 ± 283	1.9 ± 0.02
Breakneck Creek (BN)	0.29 ± 0.07	10,200 ± 550	3,500 ± 830	1,900 ± 250	595 ± 77	3,290 ± 128	2.7 ± 0.07
Robinson Run (RR)	0.01 ± 0.003	7,950 ± 360	3,550 ± 330	480 ± 50	157 ± 14	2,270 ± 138	0.4 ± 0.01
Little Sugar Creek (LS)	0.01 ± 0.003	8,400 ± 1,150	815 ± 120	360 ± 70	389 ± 47	1,860 ± 278	1.8 ± 0.4
Little Miami River (LM)	1.91 ± 0.34	8,500 ± 430	n.d.	n.d.	292 ± 12	3,250 ± 48	2.7 ± 0.1

n.d. = not determined

Table 2. Sediment particle size distribution

Sediment particle size characteristics from laser particle analysis (mean ± std. deviation)

Location	% Clay	% Silt	% Sand	% Gravel	Specific surface area (μm^2)	D_{50} (μm)
TK	2.8 ± 0.01	30.5 ± 0.5	63.7 ± 0.4	3.1 ± 0.4	0.090 ± 0.001	142.3
PM	2.3 ± 0.1	32.7 ± 0.1	60.2 ± 0.3	4.8 ± 0.8	0.086 ± 0.003	167.7
BN	2.5 ± 0.1	30.2 ± 1.2	55.7 ± 2.3	11.7 ± 3.5	0.083 ± 0.003	168.8
RR	0.2 ± 0.001	2.6 ± 0.03	85.1 ± 0.7	12.2 ± 0.7	0.014 ± 0.001	309.8
LS	n.d.	0.5 ± 0.1[a]	98.9 ± 0.1[a]	0.6 ± 0.1[a]	n.d.	1250[a]

n.d. = not determined; [a] Particle size determined with stacked sieves

Experimental design

The nickel partitioning experiment was performed under three overlying water pH conditions (pH 5, 7 or 9) and three overlying water Ni concentrations (0.5, 2 or 5 mg L^{-1}). Each treatment was replicated six times (n = 54 jars per sediment type) to allow for destructive sampling after 0, 1, 4, 7, 14 and 28 days of Ni addition. Buffer solutions made with reconstituted freshwater

(OECD 2007) were used to reach the pH of interest in each treatment (Table A1). We used a modification of OECD method 308 (OECD 2002) to measure Ni partitioning and removal in field-collected oxic sediments. Septa jars (250 mL, Figure 1) were filled with wet sediment aliquots (sediment layer of ~2 cm, 84±1 g) and 120 ml of the respective buffer solution (water:sediment volume ratio 4:1), and were allowed to equilibrate for 10 days at 20ºC to reestablish natural vertical redox gradients. The septa jars were continuously aerated with an aquarium pump and manifold and the water level was monitored daily for evaporation. When necessary to account for evaporation, reagent-grade water (resistivity > 18 MΩ-cm) was added up to the initial volume of the overlying water. Following the 10-d equilibration period, nickel stock solution was added to the overlying water of each septa jar to reach the target concentration of dissolved Ni in each treatment. Buffer solution controls (without sediment) for each treatment combination were set up at the same time and received Ni dosing. The buffer-only jars were not aerated to avoid evaporative loss. The data from these jars was used to account for any nickel precipitation in the buffers during incubation.

On each sampling day, septa jars for each treatment combination ([Ni] × pH) were destructively sampled (n = 9 per sampling day). Overlaying water samples were filtered through a 0.45 µm polyether sulfone (PES) syringe filter, acidified to 2% with HNO_3, and stored in 15 mL centrifuge tubes until further analysis. At the same time, water was removed from the buffer-only controls, filtered, and stored until further analysis. All of the sediment within each jar was collected using a plastic spoon, stored in polyethylene bags (Whirl-pak®), manually homogenized, and stored in the freezer (-18ºC) prior to geochemical analyses. Any loose microbial biomass that developed on the sediment surface throughout the experiment was disposed of prior to sediment sampling. The same experimental procedure was repeated for all five sediment types, except for the TK experiment that used different buffer systems than the other four sediment types (Table A1). In addition to the Ni partitioning assays, an experiment following the same set-up and methodology was performed to compare Ni sorption to sorption of Fe and Al to bedded sediment. For this study, we used only LS and LM sediments at pH 7 and dosed separately with Ni, Fe, or Al at 2 mg L^{-1}.For this metal comparison study, only overlying water was sampled and sediments were discarded.

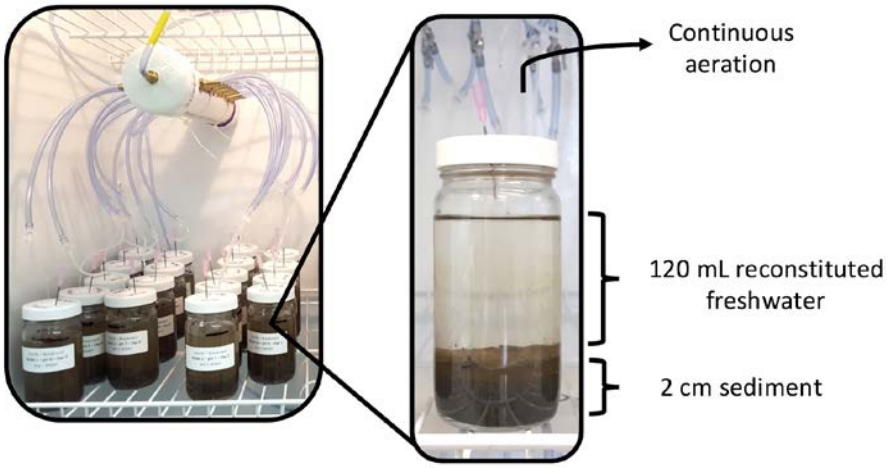

Figure 1. Images of the experimental setup for incubating sediment.

Sediment & water chemistry analyses

Filtered overlying water samples were analyzed via inductively-coupled plasma optical emission spectroscopy (ICP-OES) for dissolved Fe and Ni concentrations. Sediment samples were analyzed for particle size, organic matter content, total and oxidized metal concentrations, and AVS concentration. Particle size was obtained by running dry homogenized sediment samples through a Malvern Mastersizer 2000 Laser Particle Size Analyzer, which uses sonication and laser beams to separate and measure particle size. Organic matter (OM) content was determined as loss-on-ignition (500ºC for 4 hours). Total metal concentrations (Al, Fe, Mn, and Ni) were obtained through sediment digestion in concentrated nitric acid at reflux temperatures (HotBlock). The digested samples were then allowed to settle overnight and diluted with reagent-grade water prior to analysis by ICP-OES. For oxidized Fe and Mn and associated metals, selective extractions (Kostka and Luther 1994) were used to differentiate between the amorphous (ascorbate) and total oxidized minerals (dithionite). The extracts were centrifuged and filtered, and metal concentrations in supernatant were determined by ICP-OES. Acid volatile sulfide (AVS) analysis was performed using methodology and setup described by Allen and colleagues (Allen et al. 1993). Briefly, sediment aliquots were acidified with hydrochloric acid (to 1 M) and NaOH-filled impingers served as traps to capture any released. Sulfide concentrations were measured through colorimetric spectrometry after reaction with mixed diamine reagent. All analyses were completed with appropriate quality assurance/quality control checks (Table A2), which included blanks, duplicates, and a standard reference material (total metals only, Domestic Sludge, NIST SRM 2781).

Statistical analyses

The adsorption of Ni to sediment during incubations were modeled from the loss of Ni from overlying water using both pseudo first- (Eq. 1) and pseudo second-order (Eq. 2) kinetic equations (Jain et al. 2004, Kumar 2006).

$$Ni_t = Ni_e \cdot \left(1 - e^{-k_1 \cdot t}\right) \quad \text{(Eq. 1)}$$

$$Ni_t = \frac{k_2 \cdot {Ni_e}^2 \cdot t}{1 + k_2 \cdot Ni_e \cdot t} \quad \text{(Eq. 2)}$$

Ni_t and Ni_e are coTncentrations of Ni sorbed to sediment at time *t* and equilibrium respectively, and k_1 and k_2 are the pseudo first- and pseudo second-order rate constants. Ni_t was calculated as the difference between Ni concentrations remaining in solution at time *t* and the initial concentration of Ni, corrected for volume of buffer and mass of sediment in the jars (i.e., $Ni_{t=0}$ - $[Ni]_t$ × buffer volume/sediment dry mass). Kinetic equations were fit to the data using non-linear least squares regression. Pseudo first- and second-order model fits were compared using R^2 of the relationship between model fits and measured Ni concentrations. With the exception of one treatment combination (RR sediment, pH = 5, Ni = 0.5), Ni sorption kinetics could be significantly explained by the selected models, and in many cases the proportion of the variance explained was large (i.e., $R^2 > 0.90$). Parameters extracted from the model fits (Ni_e and k) were used for subsequent data analyses. The pH 5 buffer used during the TK sediment assay was highly unstable and these data were excluded from analysis.

Given the expected importance of Fe for Ni binding in these sediments, a hydrous ferric oxide-specific Ni binding rate ($K_{Ni\text{-}HFO}$) was calculated according to Campbell and Tessier (1996) and Tessier (1992):

$$K_{Ni-HFO} = \frac{Ni_{HFO}}{Fe_{HFO} \cdot [Ni]}$$

where Ni_{HFO} and Fe_{HFO} are concentrations in the ascorbate extraction (μg g^{-1}), and [Ni] is the dissolved Ni concentration (mol L^{-1}). Fe and Ni concentrations from ascorbate extractions were measured at each sampling time, and the amount of Ni in the ascorbate extraction increased through time to a threshold concentration. The $K_{Ni\text{-}HFO}$ at equilibrium was estimated by fitting the temporally-resolved data to a Michaelis–Menten saturating function (example in Figure 4):

$$[K_{Ni-HFO}]_t = \frac{[K_{Ni-HFO}]_e \cdot t}{b + t}$$

where $[K_{Ni\text{-}HFO}]_e$ is the partitioning coefficient at equilibrium, *t* is the time since metal addition, and *b* is the half saturation constant.

To compare Ni sorption among sediments, parameters describing Ni sorption kinetics (i.e., Ni_e as a proportion of added Ni, time to 70% removal, k_2) were correlated to bulk sediment characteristics. Correlations were completed separately for different overlying water pH due to the observed differences in kinetics between pH treatments. The strength of linear correlations between kinetic and sediment variables was calculated as Pearson's *r* correlation coefficients. All analyses were completed in R (version 3.3.2) using the nls function for non-linear least squares regression (R Core Team 2015). All values presented in the text are means ± standard deviation unless otherwise noted.

Results & Discussion

Sediment and water chemistry

Field-collected sediments differed in key geochemical characteristics (i.e., particle size, organic matter content, oxidized Fe, and AVS), especially between sandy (RR and LS) and fine (TK, PM, and BN) sediments (Tables 1 & 2). Median particle diameter (D_{50}) and particle size distribution were consistent among TK, PM, and BN sediments, with silt accounting for 30% of particles and sand composing nearly 60% of sediment samples. RR and LS sediments were sandier (Sand = 85.1 ± 0.7% and 98.9 ± 0.1%, respectively) and had up to 7× larger D_{50} than TK, PM and BN. OM content was highest in TK and BN sediments (3.1 ± 0.3% and 2.7 ± 0.07%, respectively), which had on average 30% greater OM than PM and LS samples, and nearly two orders of magnitude higher OM than RR sediments (0.04 ± 0.01%). Although total Fe concentrations varied between 8,000–13,000 mg kg^{-1} from lowest (RR) to highest (TK) concentrations, greater differences were observed for oxidized Fe (amorphous (Fe_{HFO}) and crystalline (Fe_{CFO}) minerals) among sediment types. Specifically, LS had on average 85% less Fe_{CFO} than all other sediments, while both LS and RR showed a similar decrease in Fe_{HFO} when compared to TK, PM and BN (range 360–3,000 μg g^{-1}). TK and PM sediments had substantially higher AVS concentrations than BN, RR, and LS (nearly 10× greater than BN, >100× than RR and LS). Although the AVS concentration for TK and PM exceeded 1 μmol g^{-1} dw, the highest

observed AVS concentration in all of our samples would still only be able to account for a maximum of 16% of the observed Ni binding even at the lowest mass of Ni added (0.5 mg L^{-1}).

Throughout the experiment, pH in the pH 7 and pH 9 buffering systems (Table A1) were stable in all sediment types (pH 7 = 7.6 ± 0.3, pH 9 = 8.9 ± 0.3) and buffer-only treatments (pH 7 = 7.0 ± 0.0, pH 9 = 9.2 ± 0.3). The pH in both pH 5 buffering systems was stable in control samples (5.1 ± 0.1), but stability varied between sediment types. PM, BN, and RR had on average a slightly higher but stable pH throughout the experiment (5.8 ± 0.3), whereas pH in TK (6.3 ± 1.2) and LS (6.8 ± 0.7) overlying water were difficult to stabilize within the target range and were especially variable in TK sediment. Due to the instability of pH in pH 5 treatments of TK, those data were not included in further analyses. Analysis of buffer-only controls indicated overlying water Ni concentrations were stable in pH 5 and 7 buffers, but Ni concentrations in pH 9 buffer declined over time, especially in high Ni treatments (5 mg L^{-1}). However, it is important to note that dissolved Ni declines in pH 9 buffer were linear and most Ni precipitation occurred after majority of the sorption to sediment would have occurred (Figure 2, see Table 3 for time to 70% removal).

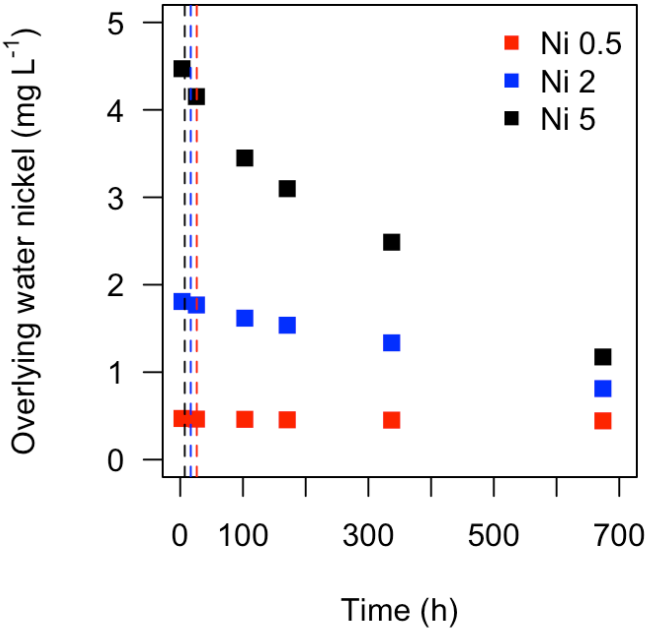

Figure 2. Overlying water Ni concentration in pH 9 buffer (sodium tetraborate/hydrochloric acid) over time for all Ni treatments. Dashed lines represent time to 70% Ni removal in Breakneck Creek sediment for each Ni treatment.

Ni sorption kinetics

Ni was removed rapidly from the overlying water and reached an equilibrium concentration within a few days (Table 3). Ni sorption was best described by pseudo second-order kinetics for most tests (29 of 42 treatments; Figure 3), but there were often minimal differences in fit between pseudo first- and second-order models. The total mass of Ni sorbed at equilibrium varied from 44–100% of the added Ni, and 29 of 42 test conditions had an Ni

Table 3. Ni sorption kinetic parameters for all sediment types

	pH treatment	Ni treatment (mg L^{-1})	Pseudo first-order			Pseudo second-order			For best model	
			Ni_e (µg g^{-1})	k_1 (h^{-1})	R^2	Ni_e (µg g^{-1})	k_2 (g µg^{-1} h^{-1})	R^2	Equilibrium removal (%)	Time to 70% removal (d)
Breakneck Creek	5	0.5	0.61	0.001	**0.968**	1.09	0.001	0.966	71	164
	7	0.5	0.38	0.035	**0982**	0.41	0.112	0.956	44	-
	9	0.5	0.65	0.051	0.981	0.69	0.122	**0.996**	80	3.6
	5	2	2.14	0.006	0.952	2.61	0.002	**0.962**	69	-
	7	2	2.60	0.055	0.975	2.73	0.035	**0.992**	72	12.5
	9	2	3.23	0.112	0.975	3.38	0.049	**0.977**	90	0.9
	5	5	5.34	0.286	0.500	5.58	0.061	**0.645**	61	-
	7	5	7.20	0.268	0.846	7.45	0.049	**0.955**	82	0.7
	9	5	8.49	0.304	0.955	8.69	0.056	**0.998**	95	0.2
Little Sugar Creek	5	0.5	0.59	0.012	0.953	0.66	0.025	**0.982**	89	9.2
	7	0.5	0.62	0.012	0.924	0.69	0.026	**0.960**	92	7.2
	9	0.5	0.66	0.049	0.978	0.70	0.114	**0.996**	94	1.5
	5	2	2.31	0.146	0.511	2.57	0.035	**0.651**	79	3.6
	7	2	2.83	0.030	0.940	3.07	0.015	**0.974**	95	2.6
	9	2	3.03	0.060	0.952	3.15	0.038	**0.982**	97	0.9
	5	5	6.61	0.012	0.811	6.76	0.004	**0.815**	86	6.2
	7	5	6.98	0.023	0.932	7.73	0.004	**0.971**	98	3.2
	9	5	7.54	0.058	0.988	7.90	0.013	**0.999**	100	0.9
Plum Creek	5	0.5	0.45	0.002	**0.927**	0.74	0.001	0.926	61	-
	7	0.5	0.32	0.013	0.930	0.37	0.042	**0.939**	50	-
	9	0.5	0.56	0.038	0.992	0.61	0.083	**0.992**	82	2.9
	5	2	1.91	0.025	**0.395**	2.15	0.013	0.364	59	-
	7	2	2.14	0.043	0.987	2.29	0.028	**0.994**	70	105
	9	2	2.82	0.046	0.989	2.98	0.026	**0.993**	92	1.7
	5	5	4.79	0.004	**0.867**	6.02	0.001	0.850	61	-
	7	5	5.71	0.028	**0.993**	6.23	0.007	0.989	72	5.0
	9	5	7.10	0.052	0.988	7.53	0.011	**0.999**	96	1.4

Table 3. cont.

	pH treatment	Ni treatment (mg L^{-1})	Pseudo first-order			Pseudo second-order			For best model	
			Ni_e (µg g^{-1})	k_1 (h^{-1})	R^2	Ni_e (µg g^{-1})	k_2 (g µg^{-1} h^{-1})	R^2	Equilibrium removal (%)	Time to 70% removal (d)
Robinson Run	5	0.5	n.s.	n.s.	0.158	n.s.	n.s.	0.127	n.s.	n.s.
	7	0.5	0.59	0.015	0.942	0.67	0.029	**0.979**	91	7.3
	9	0.5	0.67	0.055	0.983	0.71	0.124	**0.999**	96	1.3
	5	2	2.02	0.004	**0.829**	2.38	0.002	0.791	63	-
	7	2	2.76	0.036	**0.901**	2.93	0.021	0.867	85	2.0
	9	2	3.06	0.077	0.968	3.17	0.049	**0.992**	98	0.7
	5	5	5.28	0.004	**0.888**	7.10	0.000	0.881	67	-
	7	5	6.56	0.029	**0.842**	7.10	0.006	0.796	84	2.6
	9	5	7.49	0.061	0.974	7.77	0.016	**0.988**	99	0.8
Tinkers Creek	5	0.5	n.a.	n.a.	n.a.	n.a.	n.a.	n.a.	n.a.	n.a.
	7	0.5	0.50	0.015	0.956	0.57	0.034	**0.981**	60	-
	9	0.5	0.66	0.056	**0.958**	0.66	0.356	0.925	69	-
	5	2	n.a.	n.a.	n.a.	n.a.	n.a.	n.a.	n.a.	n.a.
	7	2	2.84	0.021	0.965	3.19	0.008	**0.974**	77	16.2
	9	2	3.44	0.317	0.944	3.56	0.095	**0.989**	86	0.6
	5	5	n.a.	n.a.	n.a.	n.a.	n.a.	n.a.	n.a.	n.a.
	7	5	7.36	0.021	0.990	8.19	0.003	**0.995**	81	9.2
	9	5	9.11	0.390	0.981	9.33	0.052	**0.999**	93	0.3

Ni_e = nickel equilibrium concentration; k_x = removal rate coefficient for the respective kinetics (pseudo first-order = 1, pseudo second-order =2); n.a. = not available; n.s.= non-significant model fit

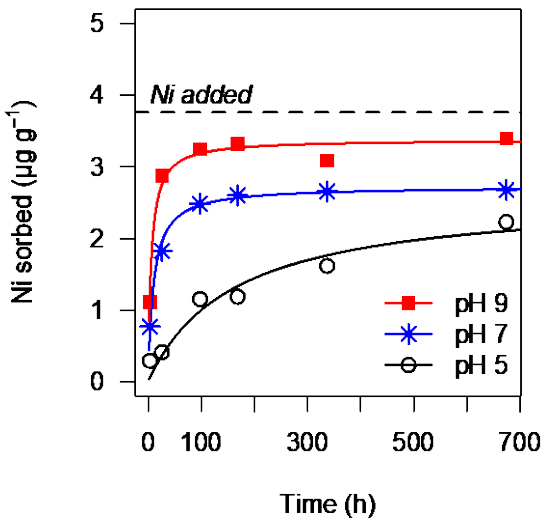

Figure 3. Example Ni kinetics when exposed to Breakneck Creek sediment (2 mg L^{-1} Ni in overlying water). Solid lines represent best-fits from a pseudo second-order kinetic model (R^2 > 0.96).

concentration at equilibrium that was predicted to remove greater than 70% of the added Ni. Sorption kinetics were rapid for most treatments; the median time predicted to remove 70% of the added Ni was just 1.5 days, and only one treatment (i.e., BN sediment, pH = 5, Ni = 0.5) was predicted to remove >70% of the added Ni, but not within the 28 day test period.

Sediment treatments that would not reach the 70% removal threshold at equilibrium were characterized by low pH and/or low added Ni. With the exception of LS sediment, treatments with overlying water at pH 5 were not able to reach the 70% removal threshold within 28 days. Equilibrium Ni concentrations at pH 5 were 79–89% of the added Ni in LS sediment, but just 59–71% of the added Ni in the remaining sediments. BN, PM, and TK sediments were not able to reach the 70% threshold at equilibrium at neutral pH and low Ni dosing (0.5 mg L^{-1}). In general, the proportion of Ni removed was greatest in the highest Ni concentration treatments (5 mg L^{-1}) and there is no evidence that this concentration of added Ni saturated binding sites.

Ni binding to metal oxide minerals

The concentration of Ni in the ascorbate extractions increased through time in all treatments, which indicates that at least some of the Ni being lost from the water column was sorbed to iron oxides (Figure 4). The $K_{Ni\text{-}HFO}$ at equilibrium was calculated for all treatments (Table 4), however some of the sediments, and especially those at pH 5, did not reach equilibrium before the experiment was terminated. Therefore, these equilibrium $K_{Ni\text{-}HFO}$ that were calculated from extrapolations beyond the experimental period should be interpreted with caution. $K_{Ni\text{-}HFO}$ at equilibrium can be interpreted as the affinity of the Fe oxides in that sediment for Ni (Campbell and Tessier 1996). $K_{Ni\text{-}HFO}$ measured here varied significantly among sediment types ($p = 0.0002$) and were within the range of values measured in Canadian lake sediments (Tessier 1992). However, the data from Canadian lake sediments indicated a strong relationship between $K_{Ni\text{-}HFO}$ and overlying water pH, but our experimental data did not find a strong pH–K_{NiHFO} relationship ($p = 0.41$) (Figure 5). Most sediments at low pH (5–7) are close to the expected values found by Tessier (1992), but all sediments at pH 9 had Fe oxides with much

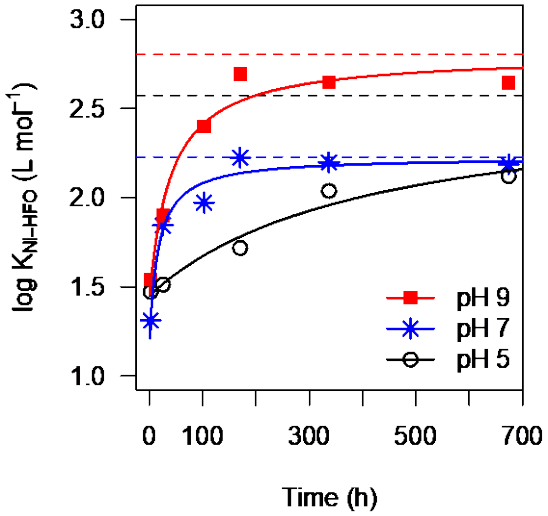

Figure 4. Increased binding of Ni to hydrous ferric oxides during incubations of Plum Creek sediment (2 mg L^{-1} Ni loading) under different overlying water pH conditions. The solid line represents the best-fit line from a saturating function, and the dashed line indicates the predicted Ni-HFO sorption constant at equilibrium ($[K_{Ni-HFO}]_e$).

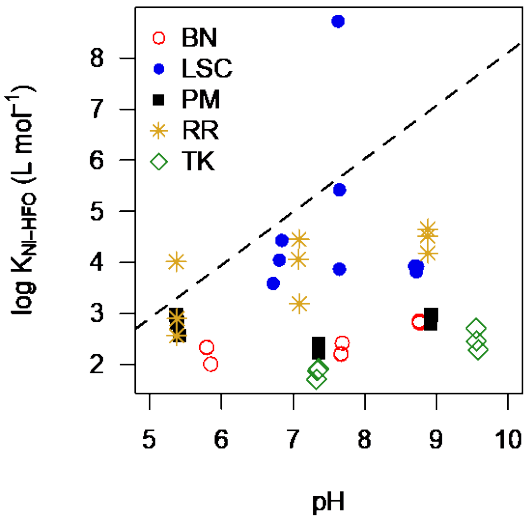

Figure 5. Relationship between the equilibrium K_{Ni-HFO} and overlying water pH. K_{Ni-HFO} was not related to pH (p = 0.41), but did differ significantly among sediment types (p = 0.0002). The dashed line indicates the predicted relationship between pH and K_{Ni-HFO} in Canadian lake sediment (Tessier 1992).

lower Ni sorption affinity than predicted (Figure 5). Most of the sediments at pH 9 had a K_{Ni-HFO} at equilibrium at the end of the experiment, and thus we do not think the lower than expected sorption affinity is related to incubation time. Lower than expected Ni-Fe sorption in pH 9 treatments may be due to increased complexation of Ni to organic matter at high pH (Tessier 1992). Correlations between Ni removal and sediment parameters (see below) offer evidence that organic matter may influence the removal of Ni at high pH. Importantly, although Ni sorption is lower than expected by Tessier (1992) at high pH, the Ni-Fe sorption at high pH was still similar or greater than sorption at circumneutral pH; therefore, there is no decline in Ni removal at high pH but just no improvement in removal.

The ascorbate reagent used in the selective extraction assays extracts all easily-reducible metals (and any sorbed metals), and thus the Ni extracted cannot be definitively linked to sorption by Fe. However, the concentration of Fe oxide minerals was an order of magnitude greater than the total concentration of Mn in these sediments and comparable to Al concentrations (Table 1). Due to the abundance of oxidized Fe minerals relative to Mn and Al, we argue that Fe minerals are the main sorbent for Ni in these natural sediments. However, this assumption should be verified with more detailed mineralogical study of these sediment (see **Future Directions**).

Comparison between Ni, Fe and Al removal rates

Incubations of Little Miami River and Little Sugar Creek sediment with Al, Fe, and Ni demonstrate the differences and similarities in uptake kinetics between metals. At pH 7, Al and Fe were very efficiently and rapidly sorbed to sediment (Table 5). For both sediments, Al and Fe sorption was both faster and more complete than sorption of Ni. Fe and Al were removed from

the overlying water to below 70% of the added metal within 6–20 minutes of addition, whereas Ni removal to the same threshold took 40–65 hours (Table 5). Although the uptake kinetics were much faster for Fe and Al, all three metals still reached the 70% removal threshold within 96 hours of addition of metal. Al and Fe were also removed more completely (98–100% removed) when compared to Ni (94–95% removal). Although Fe and Al were removed from overlying water to sediment more quickly and completely than Ni, all three metals can be removed from overlying water at sufficient rates and with a substantial efficiency such that sorption to oxidized sediments should be considered an effective sink of metal from a regulatory perspective.

Correlation of Ni removal to sediment properties

The relative amount of Ni removed from water and sorbed to sediment was correlated to many bulk sediment properties at all overlying water pH conditions (Table 6). Most notably, removal efficiency (i.e., % removed) was positively correlated to $K_{Ni\text{-}HFO}$ (Figure 6A), which intuitively indicates that sediment with HFO minerals with greater affinity for Ni can remove a greater mass of Ni. The calculation of $K_{Ni\text{-}HFO}$ includes overlying water Ni concentrations, which may be confounded with Ni sorption parameters (calculated as loss from overlying water). However Ni_{HFO}:Fe_{HFO} ratios in sediment were also strongly correlated to removal efficiency (Figure 6B), which further supports that the affinity of Fe for Ni is driving the removal of Ni from the water column. Unfortunately, the affinity of HFO for Ni (i.e., $K_{Ni\text{-}HFO}$ and Ni_{HFO}:Fe_{HFO}) and the rate of Ni removal could not be correlated to bulk Fe concentrations in intuitive relationships. For example, Ni removal efficiency was correlated to total Fe and relative concentration of amorphous and crystalline oxide minerals but the correlations coefficients were negative (Table 6), which is the opposite of our expectations. This suggests that total concentrations of Fe and oxidized Fe are not strong indicators of the sorptive potential of those minerals.

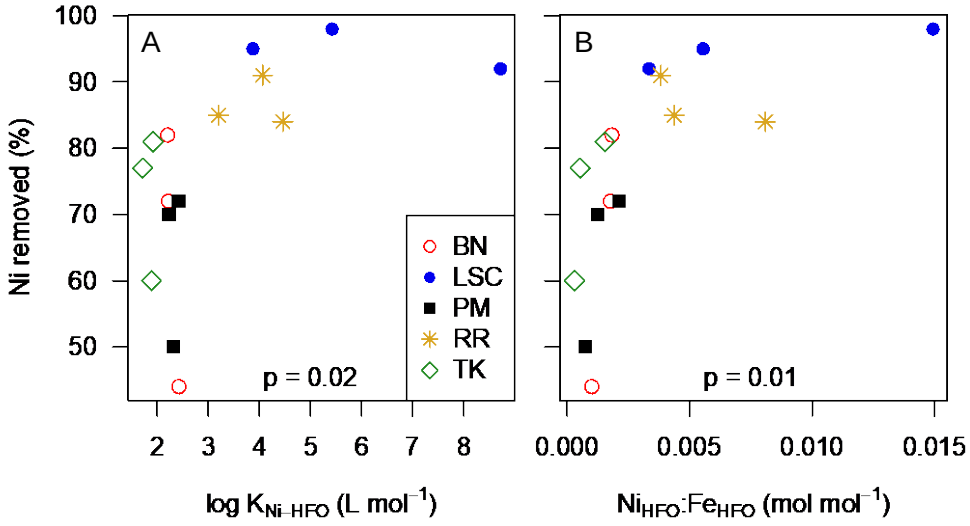

Figure 6. Ni removed at equilibrium is positively correlated to both the HFO-specific Ni sorption coefficient and the ratio of Ni:Fe extracted from HFO-specific assays. Different symbols denote different sediment types and all data are for pH 7 (pH 5 and 9 were similar).

Other bulk sediment properties that were related to removal efficiency include AVS, particle size, and organic matter (Table 6). AVS was correlated to Ni removal efficiency for pH 5 and 7

Table 4. Summary of Ni-hydrous ferric oxide partitioning coefficients ($K_{Ni\text{-}HFO}$) at equilibrium

log $K_{Ni\text{-}HFO}$ (L mol^{-1}) partitioning coefficients for each treatment combination in each sediment type

pH treatment	Ni treatment (mg L^{-1})	Tinkers Creek	Plum Creek	Breakneck Creek	Robinson Run	Little Sugar Creek
5	0.5	n.d.	2.83*	2.34	2.90	3.59
7	0.5	1.88	2.31	2.42	4.06*	8.72*
9	0.5	2.29	2.84	2.86	4.52	3.93
5	2.0	n.d.	2.57*	2.34*	4.02*	4.43*
7	2.0	1.71	2.23	2.22	3.19	3.87
9	2.0	2.46	2.80	2.83	4.18	3.82
5	5.0	n.d.	2.98*	2.01	2.56*	4.05*
7	5.0	1.92	2.42	2.20	4.46	5.42*
9	5.0	2.71	2.98	2.82	4.66*	3.92

*n.d. = not determined; * = $K_{Ni\text{-}HFO}$ did not reach equilibrium within the experimental period, and these values should be interpreted with caution*

Table 5. Al and Fe sorption kinetic parameters and comparison to Ni for Little Miami River and Little Sugar Creek

	pH treatment	Metal treatment (mg L^{-1})	Pseudo first-order			Pseudo second-order			For best model	
			Me_e (µg g^{-1})	k_1 (h^{-1})	R^2	Me_e (µg g^{-1})	k_2 (g µg^{-1} h^{-1})	R^2	Equilibrium removal (%)	Time to 70% removal (d)
Little Miami River	7	Al 2	4.05	1.531	0.769	4.05	2.365	0.825	99	0.014
	7	Fe 2	4.04	2.229	0.178	4.04	9.368	0.216	98	0.004
	7	Ni 2	3.62	0.042	0.955	3.85	0.018	0.977	94	1.711
Little Sugar Creek	7	Al 2	3.32	1.606	0.839	3.32	3.411	0.884	100	0.012
	7	Fe 2	3.29	1.770	0.754	3.29	4.921	0.768	99	0.008
	7	Ni 2	2.83	0.030	0.940	3.07	0.015	0.974	95	2.6

sediments, but the relationship was negative which indicates that sediments with greater AVS concentrations had less efficient removal of Ni. This supports previous work that demonstrated that at the sediment–water interface, Fe is more critical for controlling Ni availability than AVS. Particle size was also strongly correlated to Ni removal efficiency, though again the pattern was counterintuitive. Sediments with a larger median particle size (i.e., greater proportion of sand) had more efficient removal of Ni (Table 6, Figure 7). The importance of particle size may be related to physical limitations of Ni diffusion from the overlying water to sorption sites. Sandy sediments would be less tightly packed and allow for greater porewater–surface water exchange, thus allowing dissolved Ni in surface water greater contact with sediment sorption sites. Furthermore, sand grains are coated in metal oxides and these coated sand grains may have mineralogical properties that are related to a greater affinity for Ni. Organic matter was negatively correlated to Ni removal efficiency at pH 9 only (Table 6). As mentioned previously, under high pH, organic matter and Fe may compete for Ni sorption (Tessier 1992). Sediments with higher particulate organic matter would likely have greater dissolved organic carbon (DOC) concentrations in overlying water, which may complex Ni and decrease sorption to Fe. The suggested mechanism of complexation with DOC was not sufficiently strong to impair sorption of Ni to sediment, but rather it was strong enough to dampen the increase in sorption expected under high pH (Tessier 1992, Figure 5).

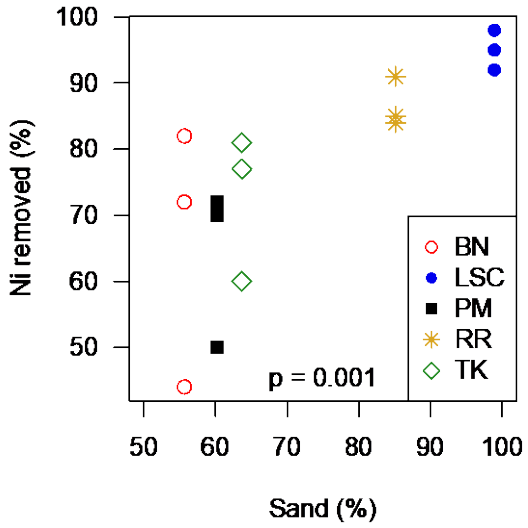

Figure 7. Ni removed at equilibrium is related to particle size and specifically is positively correlated to the proportion of sand. Different symbols denote different sediment types and all data are for pH 7 (pH 5 and 9 were similar).

The rate at which Ni reached equilibrium concentrations within the sediment (k_2) was strongly related to the pH of overlying water (Figure 8). Overlying water with a higher pH reached the equilibrium Ni concentration earlier than sediment incubated at low pH. The kinetic sorption parameters (i.e., k_2 and time to 70% removal) were not correlated to the measured sediment characteristics as strongly as removal efficiency (Table 6). Time to 70% remove was weakly correlated to $K_{Ni\text{-}HFO}$, but only in sediment at pH 7. Although this pattern matches the positive relationship between $K_{Ni\text{-}HFO}$ and Ni removal efficiency, it was not observed at pH 9.

Table 6. Summary of correlation between sediment characteristics and Ni sorption

P-values from Pearson *r* correlations between sediment characteristics and the efficiency and speed of Ni sorption. Significant correlations are in bold italics. Sign in parentheses indicates the direction of the correlation.

Variable	Equilibrium Ni conc. (% of Ni added)			Log time to 70% removal (d)			k_2 (g ug^{-1} h^{-1})		
pH	**5**	**7**	**9**	**5**	**7**	**9**	**5**	**7**	**9**
AVS	***0.048*** **(-)**	***0.04*** **(-)**	0.08	n.d.	***0.03*** **(+)**	0.52	0.46	0.67	0.74
LOI	0.92	0.12	***0.03*** **(-)**	n.d.	0.45	0.46	0.31	0.39	0.22
log(D_{50})	***0.0002*** **(+)**	***0.004*** **(+)**	***0.05*** **(+)**	n.d.	0.35	0.76	0.56	0.32	0.41
% Sand	***0.01*** **(+)**	***0.001*** **(+)**	***0.04*** **(+)**	n.d.	0.19	0.97	0.85	0.11	0.57
Total Fe	***0.04*** **(-)**	0.22	***0.02*** **(-)**	n.d.	0.39	0.16	0.64	0.90	0.07
% Fe_{HFO}	***0.01*** **(-)**	***0.004*** **(-)**	***0.01*** **(-)**	n.d.	0.15	0.80	0.67	0.46	0.28
% Fe_{CFO}	***0.0001*** **(-)**	***0.005*** **(-)**	0.09	n.d.	0.40	0.82	0.37	0.41	0.44
Fe_{HFO}:Fe_{OX}	0.66	0.17	***0.04*** **(-)**	n.d.	0.20	0.91	0.79	0.71	0.42
% Ni_{HFO}	***0.01*** **(+)**	0.23	***0.01*** **(+)**	n.d.	0.76	0.19	0.73	0.41	***0.0002*** **(-)**
% Ni_{CFO}	***0.002*** **(+)**	***0.03*** **(+)**	***0.001*** **(+)**	n.d.	0.43	0.56	0.77	0.33	***0.02*** **(-)**
Ni_{HFO}:Ni_{FeOX}	0.33	0.73	0.66	n.d.	0.64	0.06	0.43	0.81	0.15
$K_{Ni\text{-}HFO}$	0.06	***0.02*** **(+)**	***0.01*** **(+)**	n.d.	0.59	0.84	0.91	0.50	0.21
Ni_{HFO}:Fe_{HFO}	***0.01*** **(+)**	***0.01*** **(+)**	***0.01*** **(+)**	n.d.	0.23	0.75	0.97	0.14	0.13
Total Al	***0.01*** **(-)**	***0.02*** **(-)**	***0.02*** **(-)**	n.d.	0.42	0.37	0.95	0.38	0.19
Total Mn	0.26	0.34	0.14	n.d.	0.96	0.37	0.10	0.18	0.32
% Mn_{OX}	0.51	***0.001*** **(-)**	0.16	n.d.	0.48	0.88	0.34	***0.02*** **(-)**	0.33

k_2 = removal rate coefficient for pseudo first-order kinetic model; AVS = acid volatile sulfides; LOI = loss on ignition; D_{50} = median particle size diameter; Fe_{HFO} = hydrous ferric oxides; Fe_{CFO} = crystalline ferric oxides; Fe_{HFO}:Fe_{OX} = proportion of total oxidized Fe as HFO; Ni_{HFO} = Ni sorbed to hydrous ferric oxides; Ni_{CFO} = Ni sorbed to crystalline ferric oxides; Ni_{HFO}:Ni_{FeOX} = proportion of Ni bound to HFO relative to Ni bound to total oxidized Fe; $K_{Ni\text{-}HFO}$ = Ni-hydrous ferric oxide partitioning coefficients at equilibrium; Ni_{HFO}:Fe_{HFO} = Ni to Fe molar ratio on hydrous ferric oxides; Mn_{OX} = oxidized manganese; n.d. = not determined due to low n (see Table 3)

The pseudo second-order rate of Ni uptake (k_2) was correlated to the fraction of Ni bound to Fe oxides (pH 9) and the proportion of Mn as Mn oxides (pH 7). This suggests that Ni sorbed to the sediment more rapidly when a smaller proportion of that sorbed Ni was bound to oxidized Fe. Although Ni is moving rapidly into the sediment, the correlations with Ni removal efficiency suggest that a smaller proportion of Ni will ultimately be bound at equilibrium (Table 6). Overall, these data suggest that the rate of Ni uptake is determined primarily by overlying water pH, with little influence of sediment characteristics. This is in contrast to the total proportion of metal removed which is influenced both by pH and sediment characteristics.

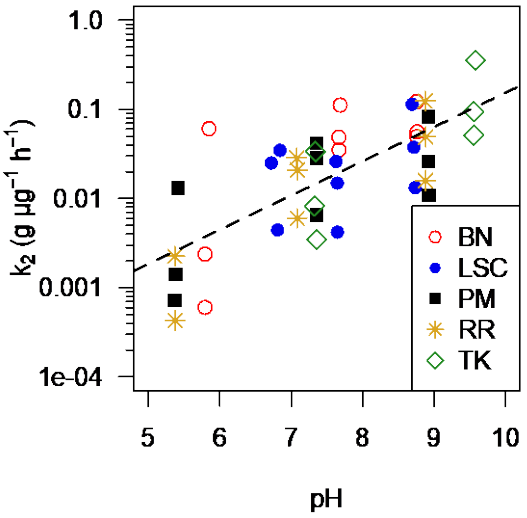

Figure 8. Relationship between overlying water pH and pseudo second-order Ni uptake rate (k_2). Different symbols denote different sediment types and the dashed line shows the best-fit line for all data.

Future Directions

Micron-scale measurement of Ni–metal oxide sorption

Determining metal speciation in sediments with a mixture of ligands is challenging using selective extraction approaches; this is especially true for metal oxide-associated metals, which simultaneously extracted multiple oxidized metal minerals (Fe, Mn, and Al) across a spectrum of crystallinity and solubility. X-ray diffraction (XRD) approaches can be used on sediment samples prepared according to our sorption methods to validate partitioning to metal oxides, determine identity of metal oxides associated with Ni, and determine the physical and chemical characteristics of the metal oxide minerals that have the strongest sorptive affinity for Ni.

Sediments from Little Sugar Creek, Robinson Run, and Plum Creek represent sediments with a broad range of Ni-HFO binding affinity (Figure 5). These sediments will be prepared in the same manner as previously (pH 7, Ni 2 mg L^{-1}) and preserved for XRD. For these samples, synchrotron based extended X-ray absorption fine structure (EXAFS) spectroscopy will be used to determine the average molecular-scale coordination environment of Ni in the sediment. X-ray microprobe analysis will be used for micron-scale spatial analysis of Ni sorption to the surface of metal oxides. This work will be done in collaboration with Dr. David Singer at Kent State University, who has substantial expertise with XRD on sediments and has previously worked at the beam at Argonne National Laboratory.

Stability of Ni-metal oxide sorption under dynamic physicochemical conditions

Sorption of metals like Ni to mineral surfaces, which is an equilibrium process, is potentially a less “permanent” change in bioavailability compared to NiS precipitation. This is concerning for regulators, as it is well known that aquatic ecosystems are not static and often go through profound changes in physicochemical conditions. Two major sediment disturbances that may alter the binding of Ni to metal oxides are resuspension of sediment and changes in sediment redox conditions. Resuspension may alter Ni-HFO sorption by placing particles with bound Ni into the water column, which may promote desorption. Furthermore, resuspension may alter the crystal structure of metal oxide minerals and change the Ni sorption affinity. Induced sediment anoxia often occurs seasonally in eutrophic freshwater ecosystems. The decline in oxygen may cause oxic and suboxic sediment layers to go anoxic, which may cause dissolution of metal oxide minerals and release of bound Ni. Our sampling and previous studies have shown that metal oxide minerals can be found in anoxic sediment, which suggests that some of these minerals have properties that make them resistant to dissolution under reducing conditions.

I propose to simulate natural disturbance on sediments that have been treated with Ni and reached equilibrium. These studies will determine how stable metal oxides are in the presence of dynamic conditions and whether the bound Ni can be desorbed. Overall, I hypothesize that Ni sorbed to metal oxides will be stable under environmentally relevant disturbance scenarios.

Resuspension. Equilibrated sediments will be resuspended for 3 hours and dissolved Ni will be measured during and after resuspension. Sediments will be allowed to re-equilibrate for ~7 days to determine if and how quickly Ni in the sediment and overlying water return to equilibrium. I hypothesize that resuspension will not release substantial Ni from the Fe-rich sediments due to the stability of metal oxides when contacted with overlying water.

Anoxia. Additional equilibrated sediments will be placed under N_2 atmosphere for 1–7 days to simulate the sediment–water interface becoming anoxic. Ni in overlying water will be measured during anoxia to estimate a rate of Ni release from metal oxide dissolution. Given that precipitation with sulfide may compensate for any desorbed Ni, we will complete these experiments with sediments that vary in their sulfur content (high AVS = Plum, low AVS = Little Sugar Creek). I hypothesize that extended anoxic periods will cause Ni to desorb, but precipitation with reduced sulfur will moderate the overlying water Ni concentrations.

References

Allen, H. E., G. Fu, and B. Deng. 1993. Analysis of acid-volatile sulfide (AVS) and simultaneously extracted metals (SEM) for the estimation of potential toxicity in aquatic sediments. *Environmental Toxicology and Chemistry* 12:1441–1453.

Campbell, P. G. C., and A. Tessier. 1996. Ecotoxicology of metals in the aquatic environment: Geochemical aspects. Pages 11–58. *in* M. C. Newman and C. H. Jagoe, editors. *Ecotoxicology: A hierarchical treatment.* CRC Press, New York, NY, USA.

Chapman, P., and F. Wang. 1998. Ecotoxicology of metals in aquatic sediments: binding and release, bioavailability, risk assessment, and remediation. *Canadian Journal of Fisheries and Aquatic Sciences* 55:2221–2243.

Costello, D. M., G. A. Burton, C. R. Hammerschmidt, E. C. Rogevich, and C. E. Schlekat. 2011. Nickel phase partitioning and toxicity in field-deployed sediments. *Environmental Science & Technology* 45:5798–5805.

Costello, D. M., C. R. Hammerschmidt, and G. A. Burton. 2016. Nickel partitioning and toxicity in sediment during aging: Variation in toxicity related to stability of metal partitioning. *Environmental Science & Technology* 50:11337–11345.

Jain, C. K., D. C. Singhal, and M. K. Sharma. 2004. Adsorption of zinc on bed sediment of River Hindon: Adsorption models and kinetics. *Journal of Hazardous Materials* 114:231–239.

Kostka, J., and G. Luther. 1994. Partitioning and speciation of solid phase iron in saltmarsh sediments. *Geochimica et Cosmochimica Acta* 58:1701–1710.

Kumar, K. V. 2006. Linear and non-linear regression analysis for the sorption kinetics of methylene blue onto activated carbon. *Journal of Hazardous Materials* 137:1538–1544.

OECD. 2002. Test No. 308: Aerobic and anaerobic transformation in aquatic sediment systems. Pages 1–19. *OECD Guidelines for the Testing of Chemicals, Section 3: Degradation and Accumulation*.

OECD. 2007. Test No. 225: Sediment-water Lumbriculus toxicity test using spiked sediment. Pages 1–31. *OECD Guidelines for the Testing of Chemicals, Section 2: Effects on Biotic Systems.*

R Core Team. 2015. R: A language and environment for statistical computing. R Foundation for Statistical Computing, Vienna, Austria.

Tessier, A. 1992. Sorption of trace elements in natural particles in oxic environments. Pages 425–453 *in* J. Buffle and H. P. van Leeuwen, editors. *Environmental Particles.* Lewis Publishers, New York, NY, USA.

Appendices

Table A1. Summary of buffer solutions physicochemistry
Physicochemical characteristics of the buffer systems used in the partitioning assays

Buffering System	Target pH	Buffering pH range	Conductivity (µS cm^{-1})	Ionic strength (mol L^{-1})
Acetic acid/sodium acetate[a]	5	3.7 – 5.6	5,450	0.09
Potassium hydrogen phthalate/ sodium hydroxide	5	4.1 – 5.9	6,670	0.11
Potassium dihydrogen orthophosphate/ sodium hydroxide	7	5.8 – 8.0	7,215	0.12
Sodium carbonate/sodium bicarbonate[a]	9	9.2 – 10.8	4,700	0.08
Sodium tetraborate/hydrochloric acid	9	8.1 – 9.2	2,560	0.04

[a] Buffering systems only used with Tinkers Creek sediment

Table A2. Analytical chemistry QA/QC
Summary of quality assurance/quality control (QA/QC) for analytical chemistry from sediment samples

Analyte	Procedural reproducibility (% relative difference)	Standard recovery (%)
Total Al	4 ± 3 (24)	42 ± 1 (8)[b]
Total Fe	6 ± 6 (24)	89 ± 3 (8)[b]
Total Mn	7 ± 6 (24)	100 ± 2 (8)[b]
Total Ni	7 ± 6 (24)	92 ± 3 (8)[b]
Ascorbate Fe[a]	6 ± 6 (30)	
Ascorbate Ni[a]	15 ± 23 (30)	
Dithionite Fe[a]	8 ± 7 (29)	
Dithionite Mn[a]	8 ± 10 (29)	
Dithionite Ni[a]	8 ± 11 (29)	
AVS	57 ± 44 (5)	
Organic matter (loss-on-ignition)	9 ± 14 (5)	
Dry weight/wet weight	4 ± 4 (5)	

[a] ascorbate and dithionite metals are from select extraction of amorphous (ascorbate) and total metals oxides (dithionite); [b] recovery of NIST standard reference material 2781